Energy Conversion and Management 85 (2014) 793–799

Contents lists available at ScienceDirect

Energy Conversion and Management

journal homepage: www.elsevier.com/locate/enconman

Numerical investigation on a thermoacoustic heat engine unit with a displacer

S. Zhang [a,b], Z.H. Wu [a,*], R.D. Zhao [a,b], W. Dai [a], E.C. Luo [a]

[a] Key Laboratory of Cryogenics, Chinese Academy of Sciences, Beijing 100190, China
[b] University of Chinese Academy of Sciences, Beijing 100049, China

ARTICLE INFO

Article history:
Available online 22 February 2014

Keywords:
Double-acting
Thermoacoustic heat engine
Displacer

ABSTRACT

A novel thermoacoustic heat engine – double-acting travelling wave thermoacoustic heat engine has been proposed by our research group recently. It consists of at least three symmetric engine and resonator units and has advantages on efficiency, power density and heat source flexibility. However, some computational and experimental results indicate a dramatic heat loss caused by the jet-flow in the thermal buffer tube due to the structures of the high temperature heat exchanger and the secondary ambient heat exchanger at its two ends. To solve this problem, a displacer locating in the thermal buffer tube is proposed to suppress the jet-flow. Moreover, the displacer is capable of isolating the hot region from room temperature, which provides an opportunity to eliminate the secondary ambient heat exchanger. In order to investigate such a double-acting thermoacoustic heat engine, a test rig of the engine unit has been developed by utilizing two linear motors to provide real operational conditions in the system. In this paper, a numerical simulation is performed to reveal the influences of the displacer on the system performance. According to the numerical results, the impact of displacer is very limited when the displacer is working under the resonant state. In addition, the influences of spring constant and mechanical damping coefficient of the displacer are analyzed in detail respectively.

© 2014 Elsevier Ltd. All rights reserved.

1. Introduction

Thermoacoustic heat engine (TAHE) is a novel kind of heat engine which can convert heat to acoustic power, i.e. mechanical energy, based on the thermoacoustic effect, such as the Sondhauss effect [1] and the Rijke effect [2]. The TAHE is mainly used to drive a Stirling type cryocooler or refrigerator or a linear alternator. Considerable attentions have been paid to develop and improve thermoacoustic heat engines (TAHE) in the past several decades, which mainly contributes to their prominent advantages. Firstly, a variety of energy sources can be used, such as solar energy and industrial waste heat. Secondly, there are no moving components within the high temperature environment capable of achieving high reliability and long life-time. Thirdly, it is environmentally friendly by using high pressure helium or nitrogen.

The TAHE based on Rijke effect, which can also be considered as convection-driven TAHE [3], has its advantage of simple design because it does not involve any heat exchangers or stack/regenerator. Zhao et al. have made their efforts to advance this kind of TAHEs to harvest thermal energy [4] and make a further application to electricity generation [5]. On the other hand, studies on transient growth of flow disturbances in a Rijke tube have given us a guidance to avoide the unwanted disturbances in triggering a Rijke tube combustion instability [6,7].

Another branch of TAHEs considered as conduction-driven TAHE [3] are based on Sondhuass effect. By introducing porous media – stack/regenerator into the tubes the gas oscillation could be enhanced considerably [1]. Based on the acoustic field distribution, this kind of TAHEs can be divided into two types – the standing-wave TAHE and the travelling-wave TAHE. In 1992, a standing-wave TAHE [8] was built by Swift with a thermal efficiency of 9%. In 2012, Smoker et al. has developed a standing wave TAHE which can convert thermal energy directly into electricity power [9]. Researchers are finding ways to lower the onset temperature of the standing wave TAHEs for better application to low-grade energy such as forced oscillation driven by loudspeaker [10]. However, due to the irreversible thermodynamic process in the stack, the standing-wave TAHE has very low thermoacoustic efficiency. On the contrary, the travelling-wave TAHE bases on the Stirling Cycle with the potential of high efficiency [11]. In 1999, Backhaus and Swift built a travelling-wave TAHE with a thermal efficiency of 30% [12]. Later in 2005, Luo et al. proposed an energy-focused travelling wave TAHE with a pressure ratio of 1.4 [13]. Zhou and Li et al. has made efforts

* Corresponding author. Tel./fax: +86 10 82543751.
E-mail address: zhhwoo@mail.ipc.ac.cn (Z.H. Wu).

http://dx.doi.org/10.1016/j.enconman.2014.01.057
0196-8904/© 2014 Elsevier Ltd. All rights reserved.

Nomenclature

Abbreviation

CM	compression motor
EM	expansion motor
TAHE	Thermoacoustic heat engine
1-D	one dimension

Symbols

A	gas area, m^2
A_s	solid area, m^2
B	magnetic field, T
c_p	isobaric heat capacity per unit mass, J/kg K
D	diameter, m
E_{net}	net acoustic power, W
E_{EM}	acoustic power consumed in expansion motor, W
E_{CM}	acoustic power input from compression motor, W
f	frequency, Hz
f_κ	spatially averaged thermal diffusion function
f_y	spatially averaged viscous diffusion function
$\dot{H}_2$	total energy power, W
i	$\sqrt{-1}$, imaginary unit
I_1	input current, A
k	thermal conductivity, W/m K
k_s	solid thermal conductivity, W/m K
K	spring constant, N/m
l	length, m
L	electrical inductance, H
M	mass of motor, kg
p_1	pressure amplitude, MPa
P_0	mean working pressure, MPa
$\dot{q}$	heat input per unit length, W/m
Q_{in}	heat transferred, W
R_e	electrical resistance, Ω
R_m	mechanical damping coefficient, N s/m
T_m	temperature, K
U_1	volume velocity, m^3/s
V_1	input voltage, V
Z_e	complex electrical impedance, Pa s/m^3
Z_m	complex mechanical impedance, Pa s/m^3

Greek symbols

γ	specific heat ratio
θ	phase delay, °
ρ	gas density, kg/m^3
σ	prandtl number
τ	transduction coefficient
ω	angular frequency, s^{-1}
Re [ ]	real part of
Im [ ]	imaginary part of
$\sim$	conjugation of a complex quantity
||	amplitude of a complex quantity

to miniaturize the travelling wave TAHE by increasing the resonant frequency and designed a 0.65 m long and 0.22 m high TAHE [14]. However, both the standing-wave TAHE and the travelling-wave TAHEs require a big long resonance tube for a good operation and have a low power density, which has greatly limited the use of these traditional TAHEs.

A analysis of a pulse tube engine, which belongs to standing wave TAHEs, was conducted [15]. The existance of the phase shifter can modulate the acoustic distribution in the engine instead of long resonant tube. Recently, our research group has proposed a novel double-acting travelling-wave TAHE [16], which consists of at least three symmetric TAHE and resonator units. TAHE units are sandwiched between two resonators. So, the resonance tubes can be shortened greatly or even eliminated. This system has advantages of power density and large capacity. However, during the researches on this system, some computational and experimental results indicate that the jet-flow in the thermal buffer tube can cause a dramatic heat loss due to the structural configuration of the high temperature heat exchanger and the secondary ambient heat exchanger at its two ends. Based on the former CFD simulation of the flow in thermal buffer tube by our research group, there is serious turbulence and mixture of hot and cold fluid inside the thermal buffer tube [17]. The jet-flow goes out of the high temperature heat exchanger can reach the secondary ambient heat exchanger and vice versa. Accordingly, the heating power is greatly wasted. For the same system in Ref. [17], experiments were conducted and the traditional method – using some mesh screen at two ends of the thermal buffer tube were adopted to suppress the jet-flow [18]. A more than 66% increase of thermal efficiency of the system was obtained when the jet-flow was suppressed. However, using mesh screen to suppress the jet-flow will consume considerable amount of acoustic power due to the resistance of the mesh screen especially for high flow velocity. And the suitable thickness of mesh screens is not easy to design and is variable to different structures of the heat exchangers. To solve this problem, a new method, locating a displacer in the thermal buffer tube, to suppress the jet-flow is proposed. In order to better understand the working mechanism of the engine with a displacer, an experimental setup is designed to investigate the engine performance, which will be introduced in this work.

2. System configuration

To suppress the heat loss caused by the jet-flow, a displacer is considered to be located in the thermal buffer tube. To study the influence of the displacer, a test unit of TAHE is designed to investigate the engine performance. Fig. 1 illustrates the schematic of the experimental setup, which consists of a compression motor (CM), a TAHE unit with a displacer and an expansion motor (EM). Both the CM and EM have two motors with dual-opposed configuration to reduce system vibration. The CM is driven by an electric

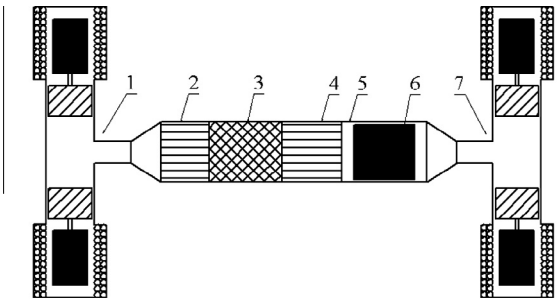

1- compression motor; 2- main ambient heat exchanger; 3- regenerator;
4- high temperature heat exchanger; 5- thermal buffer tube;
6- displacer; 7- expansion motor

Fig. 1. Schematic of the test rig of TAHE unit with a displacer.

power source, and the EM is connected with a rheostat to consume the electrical power converted by the EM from the acoustic power. The TAHE unit comprises of a main ambient heat exchanger, a regenerator, a high temperature heat exchanger, a displacer located in the thermal buffer tube. The displacer can be suspended by flexure bearing or gas bearing. Inside the displacer are located some radiation shields to reduce thermal radiation. Since the displacer can isolate heat from room temperature, the secondary ambient heat exchanger can be eliminated. Table 1 gives the dimensions of the TAHE unit. Table 2 gives the parameters of the CM and EM. Because the two motors of CM and EM are the same, only one motor's parameters are given in the table.

In this test unit, the CM and EM provide operational parameters for the TAHE unit, especially the volume velocity amplitude and phase angle. The phase angle between the pistons of CM and EM is determined by the acoustic impedances of the EM and the engine units. By changing the moving mass of the EM or the resistance of the rheostat, the phase angle can be varied within a large range. The volume velocity amplitude is mainly controlled by the electric power source. Generally, the acoustic power is inputted by the CM, amplified in the regenerator of the TAHE unit and then consumed by the EM.

3. Simulation model

The simulation is conducted using the programme of DeltaEC [19]. This programme provides a series of modules, such as DUCT, HX, STKSCREEN, et al. to simulate different thermoacoustic components. The simulation is in one dimension (1-D). The geometry parameters are given by the user. And the thermophysical properties of gas and solid properties are given in the DeltaEC's library. A shooting method is introduced in the program to satisfy a variety of boundary conditions set by the users. At the inlet of the simulation model, we set some values such as gas temperature, pressure amplitude, and input voltage as "guessed parameters" and give them initial values. By integrating the governing equations, the outlet parameters of the simulation model can be obtained. If the outlet parameters do not meet the targets, the guessed parameters will be modified and given to the inlet of the model again until the outlet parameters meet the target parameters.

Based on the classic thermoacoustic theory [20], the governing equations of the engine are:

$$\frac{dp_1}{dx} = -\frac{i\omega\rho_m}{1-f_v}\frac{U_1}{A} \tag{1}$$

$$\frac{dU_1}{dx} = -\frac{i\omega A}{\gamma p_0}[1+(\gamma-1)f_\kappa]p_1 + \frac{(f_\kappa - f_v)}{(1-f_v)(1-\sigma)}\frac{U_1}{T_m}\frac{dT_m}{dx} \tag{2}$$

$$\frac{d\dot{H}_2}{dx} = \dot{q} \tag{3}$$

$$\dot{H}_2 = \frac{1}{2}\mathrm{Re}\left[p_1\tilde{U}_1\left(1-\frac{f_\kappa-\tilde{f}_v}{(1-f_v)(1-\sigma)}\right)\right] + \frac{\rho_m c_p|U_1|^2}{2A\omega(1-\sigma^2)|1-f_v|^2}\frac{dT_m}{dx}\mathrm{Im}[f_\kappa+\sigma\tilde{f}_v] - (Ak+A_sk_s)\frac{dT_m}{dx} \tag{4}$$

Table 1
Dimensions of TAHE unit.

	D, mm	l, mm	Others
Main ambient heat exchanger	50	40	Shell-and-tube heat exchanger 223 tubes with 2 mm inner diameter
Regenerator	50	60	150 mesh stainless steel screen
High temperature heat exchanger	50	50	Parallel-plate heat exchanger Plate spacing is 1 mm
Thermal buffer tube	50	70	/
Displacer	48	50	Located in the thermal buffer tube M = 0.65 kg; K = 164.23 kN m^{-1}; R_m = 10 N sm^{-1}

Table 2
Parameters of CM and EM (single motor).

	D, mm	M, kg	K, kN m^{-1}	R_m, N s m^{-1}	R_e, Ω	Bl, N A^{-1}
CM	60	2.08	180	16	3.72	97.7
EM	50	1.1	167.5	20	3.5	95

where ω is angular frequency, P_0 represents mean pressure, f_v and f_κ are viscous function and thermal function. Other symbols are defined in Nomenclature in detail.

The acoustic power can be calculated as [20,21]

$$E = \frac{1}{2}|p_1||U_1|\cos\theta \tag{5}$$

where θ is the phase difference between p_1 and U_1. The governing equations of the CM and EM are [19]:

$$p_{1,out} - p_{1,in} = -\tau I_1 - Z_m U_1 \tag{6}$$

$$V_1 = Z_e I_1 - \tau U_1 \tag{7}$$

$$Z_e = R_e + i\omega L \tag{8}$$

$$Z_m = R_m/A^2 + i(\omega M - K/\omega)/A^2 \tag{9}$$

$$\tau = Bl/A \tag{10}$$

where $p_{1,out}$, $p_{1,in}$ are the pressure amplitudes at the back and front interfaces of the piston, respectively, Z_m is the complex mechanical impedance, Z_e is the complex electrical impedance, R_e is the electrical resistance of the coil. L is the electrical inductance of the coil, and we balance L with an external electrical compliance, hence L is 0 here. R_m is the mechanical damping coefficient. For CM, V_1 is guessed to meet the target of 6 mm displacement amplitude of the EM piston. For EM, V_1 is 0.

And the governing equations of the displacer are [19]:

$$p_{1,out} = p_{1,in} - \left[\frac{R_m}{A^2} + \frac{i(\omega M - K/\omega)}{A^2}\right]U_1 \tag{11}$$

The net acoustic power E_{net} generated by the TAHE unit is:

$$E_{net} = E_{EM} - E_{CM} \tag{12}$$

where E_{EM} is the acoustic power consumed in the EM and E_{CM} is the acoustic power input from the CM.

And the thermoacoustic efficiency of the TAHE unit is:

$$\eta = \frac{E_{net}}{Q_{in}} \times 100\% \tag{13}$$

where Q_{in} is the heat input in the heater.

In the simulation, f is set as 80 Hz. p_m is set as 4.0 MPa. The ambient temperature is 20 °C, and the heating temperature is 650 °C. The displacement amplitude of the EM motor is set as 6 mm.

4. Simulation results and discussions

Our research group has previously studied a similar test rig based on the above-mentioned simulation model [18]. In the pre-

vious study, the system consists of a CM, a TAHE unit and an EM, without a displacer. The previous TAHE unit has a secondary ambient heat exchanger other than the components consists in the current system. The dimensions of the same components in the TAHE unit are same. The simulation results and the experimental results have a very good agreement. The error of net acoustic power between simulation and experiment is less than 6%. Although the numerical thermal efficiency is a little higher than the experimental thermal efficiency, the needed external resistance when the peak is achieved coincides perfectly. Consequently, we believe that the above-mentioned simulation model can simulate the real conditions well.

Based on the above-mentioned simulation model, the simulation results are discussed in this section. Firstly, the comparison between the TAHE units with and without the displacer is made. Then, influences of the spring constant and mechanical damping coefficient of the displacer are studied.

4.1. Displacer with resonant state

First of all, the influence of the displacer on the system performance is most concerned. So, a comparison between the TAHE units with and without the displacer is made. In the TAHE unit with the displacer, the 50 mm-long displacer is located in a 70 mm-long thermal buffer tube. A special resonant state of the displacer is investigated. In order to maintain the same volume, The TAHE unit without a displacer has a 20 mm-long thermal buffer tube and has no secondary ambient heat exchanger. It is noted that in one-dimension simulation the influence of jet-flow is ignored. As mentioned above, the CM and EM work together to provide operational conditions for the TAHE unit. One of the most common methods is to change the external resistance and the moving mass of the EM. Here, the external resistance of EM is changing to realize the different phase angle conditions.

Figs. 2–5 demonstrate the influence of the displacer. The phase difference of volume velocity between the two ends of the TAHE unit is vital to the performance of the thermoacoustic engine. In the double-acting thermoacoustic engines, the phase difference is $-120°$ for three-cylinder system and $-90°$ for four-cylinder system [22]. The curves of phase difference of volume velocities are shown in Fig. 2. The dash curve shows the phase difference between CM and EM with the displacer and the solid curve shows it without the displacer. The two curves are quite close, which means a very little effect on the phase difference between CM and EM when the displacer is oscillating resonantly. A $-120°$ phase difference between CM and EM is achieved when the external resistance is 97 Ω. Similarly, in Fig. 3, the curves of volume velocities of CM when there is a displacer and no displacer are almost coincident. The curves of thermoacoustic efficiency and net acoustic power

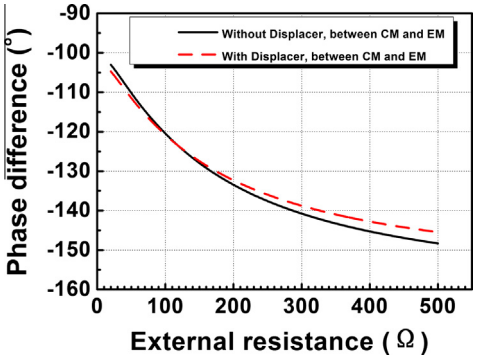

Fig. 2. The influence of displacer on the phase difference of volume velocity between CM and EM under different external resistance.

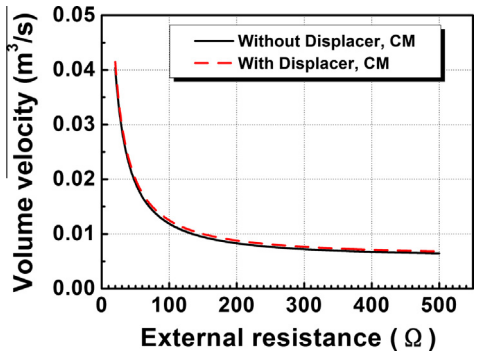

Fig. 3. The influence of displacer on the volume velocity at CM under different external resistance.

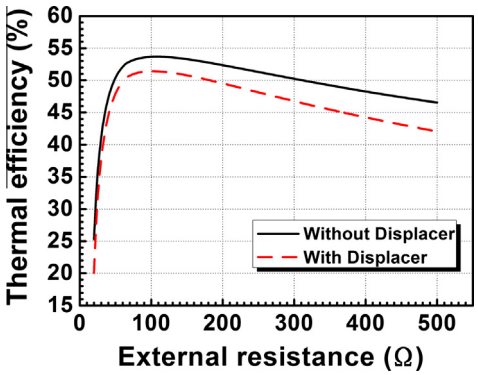

Fig. 4. The influence of displacer on the thermal efficiency under different external resistance.

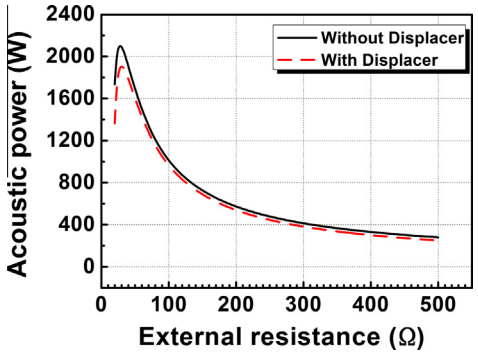

Fig. 5. The influence of displacer on the acoustic power under different external resistance.

generated in the TAHE unit are shown in Figs. 4 and 5. Although, the displacer dissipates small amount of acoustic power and reduces the efficiency because of the mechanical damping loss, the loss of the displacer is acceptable. Additionally, it is worth noting that the cross-sectional averaged model cannot simulate the heat loss caused by the jet-flow effect in the thermal buffer tube, the engine performance with the thermal buffer tube may be greatly overestimated. However, this heat loss can be completely suppressed by the displacer.

4.2. The influence of spring constant of the displacer

So far, we know that the displacer in resonant state has a little negative influence on the system performance. Actually, a displacer with non-resonant state is more common in the real system.

According to Eq. (11), $\omega M - K/\omega = 0$ when the displacer oscillates resonantly. The resonant frequency is 80 Hz and the mass of the displacer is 0.65 kg. Hence the spring constant should be 164.23 kN m^{-1}. Here, four spring constants are adopted, which are 0, 82.12 kN m^{-1}, 164.23 kN m^{-1} and 328.46 kN m^{-1}. Zero spring constant represents the displacer supported by the gas bearing. A spring constant of 82.12 kN m^{-1} reflects an inertial impedance characteristic of the displacer. A spring constant of 328.46 kN m^{-1} reflects a capacitive impedance characteristic of the displacer.

Figs. 6–9 show the influence of the spring constant. The curves of phase difference of volume velocity between CM and EM are shown in Fig. 6. The spring constant has a large influence on the phase difference. A −120° phase difference between CM and EM is obtained when the spring constant near 164.23 kN m^{-1}, which is the resonant state. And at this point, the external resistance is 95 Ω. When the spring constant is lower, the external resistance has weaker regulation ability on the phase difference. In Fig. 7, the dash-dot-dot lines represent the volume velocities of displacer when the spring constant are 328.46 kN m^{-1},164.23 kN m^{-1}, 82.12 kN m^{-1} and 0, respectively. These four curves are almost coincident. And the other four lines are the volume velocities of CM with four different spring constant. Only when the spring constant is 164.23 kN m^{-1}, that is when the displacer oscillates resonantly, the volume velocities of displacer and CM are able to be equal. Here the external resistance is 373 Ω, and the volume velocity of CM and displacer is 7.23×10^{-3} m^3/s.

The net acoustic power generated in TAHE and thermal efficiency are given in Figs. 8 and 9. According to the trend shown in the figures, there is a maximum value of thermal efficiency and a maximum value of net acoustic power. When the spring constants are 0 and 82.12 kN m^{-1}, the maximum net acoustic power has not yet been obtained within the threshold of external resistant. And when the spring constants are 328.46 kN m^{-1} and 164.23 kN m^{-1}, a smaller spring constant results in a larger maximum net acoustic power and a smaller external resistance being needed. Although the maximum values of net acoustic power are not obtained when the spring constants are 0 and 82.12 kN m^{-1} in the threshold of external resistance, trend can be predicted that smaller spring constant is benefit for higher acoustic power. In the current simulation condition, the maximum net acoustic power of 2852.4 W is achieved when the spring constant is 0 and the external resistance is 20 Ω. With the decrease of the spring constant, the maximum thermal efficiency is increasing, reaches highest at the resonant state, and decreases again. The external resistance required for the maximum thermal efficiency is increasing with the increase of spring constant. The maximum thermal efficiency is 51.41% when the spring constant is 164.23 kN m^{-1} and external resistance is 102 Ω.

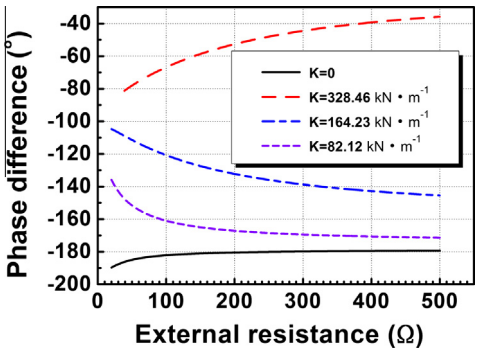

Fig. 6. The influence of spring constant on the phase difference of volume velocity between CM and EM under different external resistance.

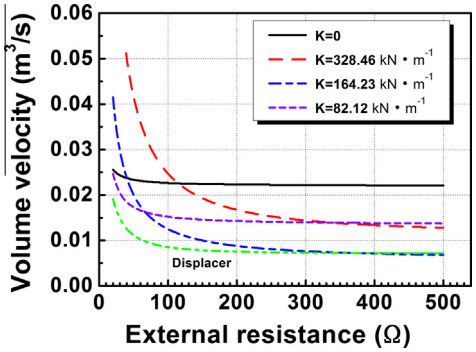

Fig. 7. The influence of spring constant on the volume velocity under different external resistance.

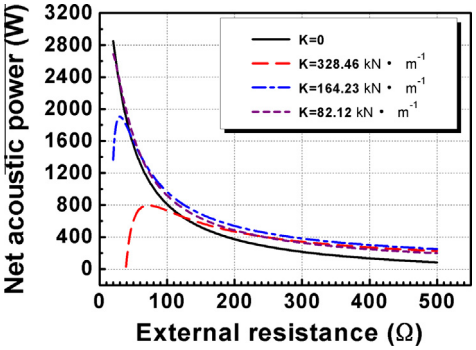

Fig. 8. The influence of spring constant on the acoustic power under different external resistance.

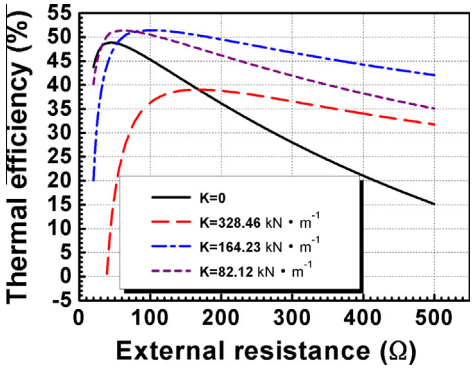

Fig. 9. The influence of spring constant on the thermal efficiency under different external resistance.

4.3. The influence of mechanical damping coefficient of the displacer

Other than the spring constant, the mechanical damping coefficient of the displacer is also a dominant parameter that will influence the performance of the test rig. Hence in this section, the influence of mechanical damping coefficient is mainly studied. The spring constant is 164.23 kN m^{-1} in this section. The mechanical damping coefficient are 0, 10 N s/m, 20 N s/m and 30 N s/m respectively.

The simulation results are given in Figs. 10–13. The influence of mechanical damping coefficient on the phase difference is modest. A −120° phase difference between CM and EM is achieved at 97 Ω, 95 Ω, 93 Ω and 91 Ω when the mechanical damping coefficient are 0, 10 N s/m, 20 N s/m and 30 N s/m respectively, according to Fig. 10. The external resistance has stronger regulation ability when the mechanical damping coefficient is smaller. The volume

velocities of the displacer with four different mechanical damping coefficients are represented by the dash-dot-dot lines, shown in Fig. 11. And these four curves are almost coincident. The other four curves shown in the figure represent the volume velocities of the CM with four different mechanical damping coefficients. A higher mechanical damping coefficient results in a higher volume velocity of CM. When the mechanical damping coefficient is 0 and 10 N s/m, the volume velocity of CM and of displacer can be equal. The external resistance needed are 282 Ω and 373 Ω, and the equal volume velocity are 7.34×10^{-3} m^3/s and 7.23×10^{-3} m^3/s. A higher mechanical damping coefficient will cause more acoustic power dissipated by the displacer. Hence the smaller the mechanical damping coefficient is, the higher the thermal efficiency and net acoustic power are (see Figs. 12 and 13).

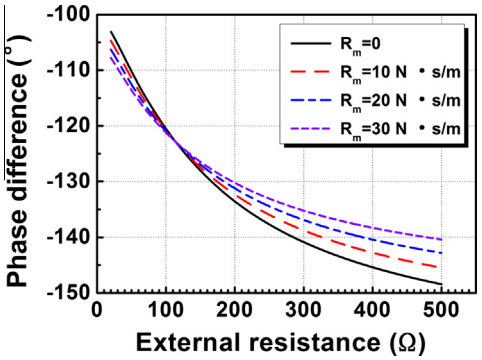

Fig. 10. The influence of mechanical damping coefficient on the phase difference of volume velocity between CM and EM under different external resistance.

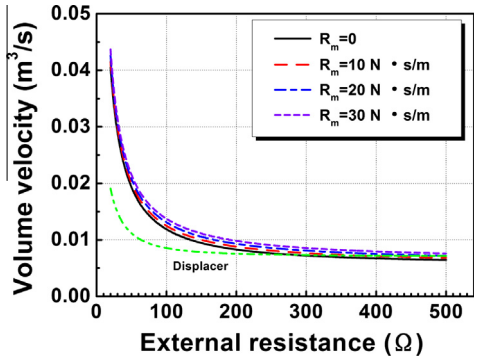

Fig. 11. The influence of mechanical damping coefficient on the volume velocity under different external resistance.

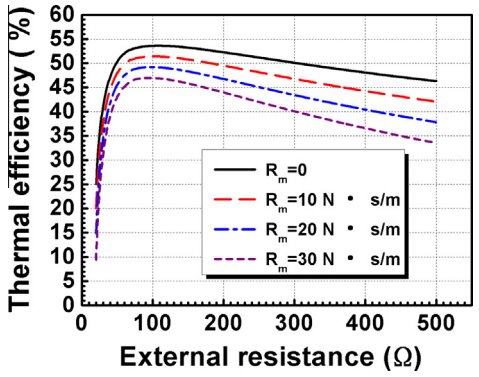

Fig. 12. The influence of mechanical damping coefficient on the thermal efficiency under different external resistance.

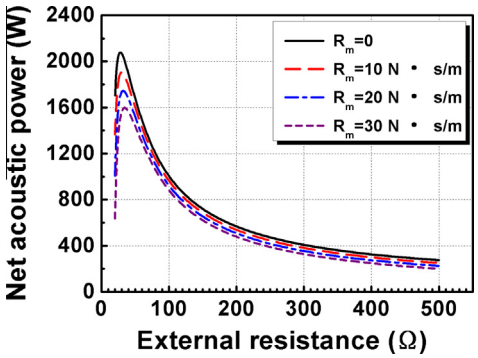

Fig. 13. The influence of mechanical damping coefficient on the acoustic power under different external resistance.

5. Conclusions

A novel double-acting travelling-wave TAHE has been proposed by our research group recently. And some research has revealed that the jet-flow in the thermal buffer tube can cause a dramatic heat loss. Consequently, a new method, locating a displacer in the thermal buffer tube, to suppress the jet-flow is presented. In this paper, a test unit is designed and simulated to study the influence of displacer. Firstly, a comparison is made between TAHE units with and without a displacer. When the displacer is oscillating resonantly, it only causes limited unfavourable losses. Secondly, the influence of spring constant of the displacer is studied. The spring constant has a significant influence on the performance of the test rig. The highest peak of thermal efficiency is obtained when the displacer is at the resonant state. Although the peaks of net acoustic power are not obtained when the spring constants are 0 and 82.12 kN m^{-1} in the threshold of external resistance, trend can be predicted that smaller spring constant is benefit for higher acoustic power. Comprehensively speaking the resonant oscillation of the spring constant is preferred. Thirdly, the mechanical damping coefficient will determine the acoustic power dissipated by the displacer. A smaller mechanical damping coefficient will achieve a better system performance. The experimental work will be performed and reported in the future.

Acknowledgments

This work was financially supported by the National Natural Sciences Foundation of China (51276186), the Major State Basic Research Development Program of China (2010CB227303), and Beijing Natural Science Foundation (3132034).

References

[1] Feldman KT. Review of the literature on Sondhauss thermoacoustic phenomena. J Sound Vib 1968;7(1):71–82.
[2] Feldman KT. Review of the literature on Rijke thermoacoustic phenomena. J Sound Vib 1968;7(1):83–9.
[3] Raun RL, Beckstead MW, Finlinson JC, Brooks KP. A review of Rijke tubes, Rijke burners and related devices. Prog Energy Combust Sci 1993;19(4):313–64.
[4] Zhao D, Chew Y. Energy harvesting from a convection-driven Rijke-Zhao thermoacoustic engine. J Appl Phys 2012;112:87–97.
[5] Zhao D. Waste thermal energy harvesting from a convection-driven Rijke-Zhao thermo-acoustic-piezo system. Energy Convers Manage 2013;66(4):87–97.
[6] Zhao D. Transient growth of flow disturbances in triggering a Rijke tube combustion instability. Combust Flame 2012;159:2126–37.
[7] Zhao D. Thermoacoustic instability of a laminar premixed flame in Rijke tube with a hydrodynamic region. J Sound Vib 2013;332(4):3419–37.

[8] Swift G. Analysis and performance of a large thermoacoustic engine. J Acoust Soc Am 1992;92(3):1551–63.
[9] Smoker J, Nouh M, Aldraihem O, Baz A. Energy harvesting from a standing wave thermoacoustic-piezoelectric resonator. J Appl Phys 2012;111:104901.
[10] Pan N, Shen C, Wang S. Experimental study on forced thermoacoustic oscillation driven by loudspeaker. Energy Convers Manage 2013;65:84–91.
[11] Ceperley P. Gain and efficiency of a short traveling wave heat engine. J Acoustic Soc Am 1985;77:1239–44.
[12] Backhaus S, Swift G. A thermoacoustic Stirling heat engine. Nature 1999;399:335–8.
[13] Luo EC, Ling H, Dai W, Zhang Y. A high pressure-ratio, energy-focused thermoacoustic heat engine with a tapered resonator. Chin Sci Bull 2005;50(3):284–6.
[14] Zhou G, Li Q, Li ZY, Li Q. A miniature thermoacoustic Stirling engine. Energy Convers Manage 2008;49(6):1785–92.
[15] Moldenhauer S, Thess A, Holtmann C. Fernandez Aballi CF. Thermodynamic analysis of a pulse tube engine. Energy Convers Manage 2012;65:810–8.
[16] Luo EC, Hu JY, Dai W, Wu ZH, Yu GY, Li HB. A double-acting single-stage travelling-wave thermoacoustic system (in Chinese). Chinese Invention Patent 2011; 201110101971.
[17] Chen YY, Zhao RD, Wu ZH, Dai W, Luo EC. CFD simulation of the double-acting thermoacoustic prime mover. In: The 26th international conference on efficiency, cost, optimization, simulation and environmental impact of energy systems; 2013.
[18] Zhao RD. Studies on the thermoacoustic conversion characteristic of double-acting thermoacoustic heat engine (in Chinese). Ph.D. thesis; 2013.
[19] Ward B, Clark J, Swift G. Design environment for low-amplitude thermoacoustic energy conversion, DELTAEC Version 6.2 Users Guide. Los Alamos, the US: Los Alamos National Laboratory; 2008.
[20] Swift G. Thermoacoustics: a unifying perspective for some engines and refrigerators. New York: AIP Press; 2002.
[21] Li S, Zhao D. Heat flux and acoustic power in a convection-driven T-shaped Thermoacoustic system. Energy Convers Manage 2013;75:336–47.
[22] Berchowitz D, Kwon Y. Multiple-cylinder, free piston, alpha configured Stirling engines and heat pumps with stepped pistons. United States Patent 2007; 7171811B1.